Characterization of the Structure of RAMP1 by Mutagenesis and Molecular Modeling

John Simms,* Debbie L. Hay,† Mark Wheatley,‡ and David R. Poyner*
*School of Life and Health Sciences, Aston University, Birmingham, United Kingdom; †School of Biosciences, University of Auckland, Auckland, New Zealand; and ‡School of Biosciences, University of Birmingham, Birmingham, United Kingdom

ABSTRACT Receptor activity modifying proteins (RAMPs) are a family of single-pass transmembrane proteins that dimerize with G-protein-coupled receptors. They may alter the ligand recognition properties of the receptors (particularly for the calcitonin receptor-like receptor, CLR). Very little structural information is available about RAMPs. Here, an ab initio model has been generated for the extracellular domain of RAMP1. The disulfide bond arrangement (Cys^{27}-Cys^{82}, Cys^{40}-Cys^{72}, and Cys^{57}-Cys^{104}) was determined by site-directed mutagenesis. The secondary structure (α-helices from residues 29–51, 60–80, and 87–100) was established from a consensus of predictive routines. Using these constraints, an assemblage of 25,000 structures was constructed and these were ranked using an all-atom statistical potential. The best 1000 conformations were energy minimized. The lowest scoring model was refined by molecular dynamics simulation. To validate our strategy, the same methods were applied to three proteins of known structure; PDB:1HP8, PDB:1V54 chain H (residues 21–85), and PDB:1T0P. When compared to the crystal structures, the models had root mean-square deviations of 3.8 Å, 4.1 Å, and 4.0 Å, respectively. The model of RAMP1 suggested that Phe^{93}, Tyr^{100}, and Phe^{101} form a binding interface for CLR, whereas Trp^{74} and Phe^{92} may interact with ligands that bind to the CLR/RAMP1 heterodimer.

INTRODUCTION

G-protein-coupled receptors (GPCRs) represent one of the largest protein families within the human genome. They have a characteristic architecture, consisting of seven transmembrane (TM) helices. Ligands bind to the extracellular face of the receptor or to a pocket formed within the TM region. In contrast, G-proteins bind to the intracellular face of the receptor.

Until recently, GPCRs were considered to act essentially as monomers. However, there is now considerable evidence that many form dimers or other oligomers (1). Most attention has been focused on dimers between GPCRs, but other proteins can also be involved. These include the family of receptor activity modifying proteins (RAMPs). These were first identified as partners for the calcitonin receptor-like receptor (CLR). CLR by itself is unable to bind any ligand; however, in the presence of RAMP1 it functions as a receptor for calcitonin gene-related peptide (CGRP), whereas in the presence of RAMP2 it becomes an adrenomedullin receptor. The CLR/RAMP3 complex also preferentially binds AM, but it has a greater affinity for CGRP than CLR/RAMP2 (2). Subsequently it has been shown that RAMPs can associate with a number of other receptors, including the calcitonin, parathyroid hormone 1 and 2, vasoactive intestinal peptide/pituitary adenylate cyclase activating polypeptide ($VPAC_1$, $VPAC_2$), glucagons, and calcium-sensing GPCRs (3–5).

All three RAMPs are thought to be built around a common architecture (2,6) (Fig. 1). They have a short, intracellular C-terminus followed by a single TM region. The largest part of the protein is the extracellular domain; ~90 amino acids for RAMP1 and RAMP3, whereas for human RAMP2 this domain is 13 residues longer. All RAMPs have four conserved cysteine residues; RAMP1 and RAMP3 have an additional pair.

It seems that the N-terminus is the major determinant of ligand binding (7,8). The structure-function relationship for RAMP2 and RAMP3 have been investigated by use of protein chimeras; these have identified residues 86–92 of human RAMP2 and 59–65 of human RAMP3 as key epitopes for AM binding (9). Deletion analysis of human RAMP3 suggested that residues 91–103 formed an important epitope for CGRP binding (10). In human RAMP1, Trp^{74} is important for high-affinity binding of BIBN4096BS, a nonpeptide antagonist of CGRP; the mutation W74K substantially reduced antagonist affinity (11). There is no structural explanation for the effect of any of these mutants, and it is unclear whether the residues or epitopes make direct contact with the ligands or act indirectly to stabilize ligand binding sites. In addition, the cysteines in the N-terminus probably form disulfide bonds. Although some information has been obtained from previous studies (12), to date, there has not been any systematic mutagenesis study of their topology.

In this study we have produced mutant RAMP1 constructs which incorporate all possible pairwise combinations of Cys to Ala mutants, to determine the organization of the disulfide bond network in hRAMP1. In addition, we have produced an ab initio molecular model of RAMP1 which is entirely consistent with the mutagenesis data presented in this study

Submitted March 7, 2006, and accepted for publication March 30, 2006.

Address reprint requests to David Poyner, School of Life and Health Sciences, Aston University, Birmingham, B4 7ET UK. Tel.: 44-(0)121-204-3997; Fax: 44 (0)121-359-5142; E-mail: d.r.poyner@aston.ac.uk.

0006-3495/06/07/662/08 $2.00

doi: 10.1529/biophysj.106.084582

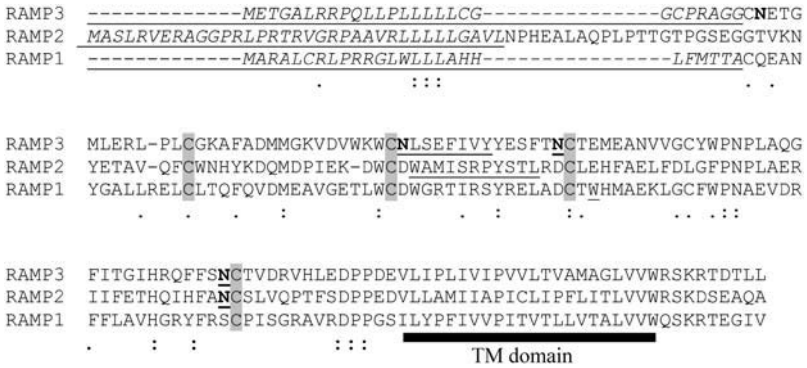

FIGURE 1 Sequence alignments of human RAMP1, RAMP2, and RAMP3. Signal peptide shown in italics and underlined; domain implicated in adrenomedullin binding shown underlined; and W, Trp^{74} required for high affinity BIBN4096BS binding. N, glycosylated residue. Conserved cysteines shaded gray. Residues labeled with a single dot are conserved in the extracellular domains of RAMP1 and RAMP3; residues labeled with two dots are conserved in the extracellular domains of all RAMPs.

and also provides a mechanistic basis for mutagenesis data previously published by other laboratories.

MATERIALS AND METHODS

Materials

Human αCGRP was from Calbiochem (Beeston, Nottingham, UK). Peptides were dissolved in distilled water and stored as aliquots at −20°C in nonstick microcentrifuge tubes (Thermo Life Sciences, Basingstoke, UK). Unless otherwise specified, chemicals were from Sigma or Fisher (Loughborough, UK). Cell culture reagents were from Gibco BRL (Paisley, Renfrewshire, UK) or Sigma. [^{125}I]-iodohistidyl^{8}-human αCGRP (2000 Ci/mmol) was from Amersham Biosciences (Chalfont, UK).

Expression constructs and mutagenesis

HA-Human CLR (hCLR) and Myc-Human RAMP1 (hRAMP1) were provided by Dr. S. M. Foord (GlaxoWellcome, Stevenage, UK) and subcloned into the vectors pcDNA3.1(−) and pcDNA3.1(+) (Invitrogen, Renfrew, UK), respectively, before mutagenesis. Mutagenesis was carried out using the QuikChange site-directed mutagenesis kit (Stratagene, Cambridge, UK), following the manufacturers instructions. Forward and reverse oligonucleotide primers were designed with single base changes to incorporate amino acid point mutations protein and to engineer restriction sites to aid screening of mutants in the final constructs. The primers were synthesized by Invitrogen.

Plasmid DNA was extracted from the cultures using a Wizard-Prep DNA extraction kit according to the manufacturer's instructions (Promega, Southampton, UK). The plasmid DNA was eluted in 100 μl sterile distilled water and stored at −20°C. Sequences were confirmed by sequencing (Functional Genomics, Birmingham, UK).

Cell culture and transfection

COS-7 cells were cultured in Dulbecco's modified Eagle's medium (DMEM) supplemented with 10% (v/v) fetal bovine serum and 5% (v/v) penicillin/streptomycin in a humidified 95% air/5% CO_2 atmosphere. For transfection, the cells were plated onto 48 well plates. Cells were transfected with 10mM polyethyleneimine (13) using 1 μg DNA per well. Characterization of expressed receptors was performed 48–72 h after transfection.

Assay of cAMP production

Growth medium was removed from the cells and replaced with serum-free DMEM containing 500 μM isobutylmethylxanthine for 30 min. αCGRP in the range 10 pM to 1 μM was added for a further 15 min. Ice-cold ethanol (95–100% v/v) was used to extract cAMP, which was subsequently measured by radio-receptor assay as previously described (14).

Secondary structure prediction

Secondary structure prediction of 16 diverse small helical, disulfide containing peptides available from the SCOP database (15) was performed using web-based versions of JPRED (16), GORIV (17), SAM T02 (18), PHD (19), PROF (20), and PSIpred (21). Each method was examined for its effectiveness at predicting the boundaries of the secondary structure obtained from the corresponding x-ray crystal structures.

Disulfide bonding prediction

Disulfide bonding patterns for 16 diverse small helical, disulfide containing peptides of known structure was performed by web-based version of DISULFIND (22), DiANNA (23), GDAP (24), DIpro (25), and PreCys (26). Each method was tested for its effectiveness at predicting disulfide bonding patterns by comparing the predicted disulfide bonding pattern to the actual disulfide bond arrangement in the corresponding x-ray crystal structure.

Ab initio prediction of the structure of RAMP1

An in-house script was used to generate an exhaustive conformational sampling set of 25,000 ab initio structures for the sequences corresponding to PDB:1HP8, PDB:1V54 chain H (residues 21–85), PDB:1T0P, and hRAMP1, using information gained from secondary structure prediction and disulfide bonding information. All structures were generated using idealized stereochemistry for all heavy atoms (N, C_α, C, and O). Side-chain orientations were modeled using SCWRL (27). Generated models were initially scored using an all-atom statistical potential (scop-e4-allatoms-x-ray-scores scoring set) as described by Samudrala and Moult (28). The ensemble of model conformations was filtered on the basis of a probability discrimination function (RADPF score), such that no more than the top 1000 models were retained for energy minimization.

Minimization was performed using a l-BFGS minimization method which utilized the AMBER all-atom force field (parm99) together with the Still GB/SA solvation model, as implemented in the TINKER (29). Minimization was performed until either convergence or a 0.1 kcal mol^{-1} cutoff point was reached. Minimized ab initio models were subsequently ranked according to the conformational free energy of the model. Further refinement of the model was performed using a molecular dynamics (MD) protocol described by Fan et al. (30). Briefly, simulations were performed in explicit water using GROMACS (31) in conjunction with the GROMOS96 43a1 force field. Simulations were preformed at constant temperature and volume in a rectangular box. Coulomb interactions were calculated using PME and van der Waal interactions with a dual cutoff (0.9 and 1.4 nm). High frequency oscillations were removed by replacing hydrogens with dummy

atoms which allowed a time step of 4 fs (32). Bonding interactions were constrained with the LINCS algorithm, whereas water molecules were constrained with SETTLE. Alternate cycles of MD simulation were performed in which the charges on the three atoms of the SPC model for water were increased by 20% followed by a further MD cycle in which the charges on the solvent were decreased by 20% (from the initial values). Each cycle consisted of 5-ns duration and 10 alternate cycles were complete making each simulation 50 ns in total. Initial ab initio model building and MD refinement was performed on Pentium IV workstations operating Linux.

Data analysis

Curve fitting was done with PRISM Graphpad 4 (Graphpad Software Inc., San Diego, CA). For cAMP studies, the data from each concentration-response curve were fitted to a sigmoidal concentration-response curve and normalized to obtain the maximum response (E_{max}) and $-\log EC_{50}$ (pEC_{50}) (Table 1). pEC_{50} and E_{max} values were compared by paired Student's *t*-test or by repeated measures one-way ANOVA followed by Tukey's test. Comparisons were only made between wild-type (WT) and mutant data from concomitantly transfected cells. A control WT experiment was included in every experiment (Table 1).

RESULTS

Computational disulfide bond prediction

To assess the effectiveness of disulfide bonding pattern prediction methods we submitted 16 sequences from the SCOP database (p8-MTCP1, frizzled cysteine-rich domain, anaphylotoxins, cytochrome *c* oxidase subunit-h categories) to web-based disulfide bonding prediction servers. For our system (small mainly helical peptides which contain disulfide bonds) the web-based neural net server DISULFIND (http://disulfind.dsi.unifi.it/) generated predicted disulfide bonding patterns which were consistent with experimental data. All cloned RAMPs were submitted to DISULFIND and the results compared. With the exception of a RAMP precursor from the genus *Tetrodon*, the predicted disulfide bonding pattern was 1–5, 2–4, and 3–6 (Fig. 2).

Secondary structure prediction

Sequences from disulfide containing small α-helical proteins (as defined above) were used to score the effectiveness of web-based secondary structure prediction methods. Of the methods selected, the SAM T02 and JPRED servers gave secondary structure predictions that were consistent with the experimentally derived structures as defined above. The sequences for all cloned RAMPs were submitted to JPRED and SAM T02 servers and the consensus prediction suggested that the extracellular portion of RAMPs was composed of three α-helical domains (helix 1, residues 29–51; helix 2, residues 60–80, and helix 3, residues 87–100 for hRAMP1, Fig. 2). A signal peptide was also identified at the proximal portion of the N-terminus (residues 1–16 hRAMP1). Furthermore, TMHMM (33) also predicted that the transmembrane domain of hRAMP1 comprised residues 118–139.

Probing the disulfide bonding pattern of RAMP1 using site-directed mutagenesis

To investigate the roles of the conserved Cys residues, each was initially substituted with Ala creating the hRAMP1

TABLE 1 Disulfide mutants of hRAMP1

hRAMP1 mutants construct	WT pEC_{50}	pEC_{50}	E_{max}
C27A	9.16 ± 0.14 (3)	9.46 ± 0.32 (3)	100 ± 3.00 (3)
C40A	9.02 ± 0.24 (3)	8.37 ± 0.12* (3)	84 ± 7.00 (3)
C57A	9.23 ± 0.28 (3)	7.99 ± 0.89*** (3)	65 ± 9.00 (3)
C72A	9.37 ± 0.19 (3)	8.55 ± 0.39* (3)	84 ± 8.00 (3)
C82A	9.24 ± 0.10 (3)	9.39 ± 0.21 (3)	92 ± 7.00 (3)
C104A	9.22 ± 0.4 (3)	8.01 ± 0.27*** (3)	70 ± 6.00 (3)
C27A–C40A	9.18 ± 0.29 (3)	>6.00 (3)	ND
C27A–C57A	9.51 ± 0.17 (3)	>6.00 (3)	ND
C27A–C72A	9.11 ± 0.65 (3)	>6.00 (3)	ND
C27A–C82A	9.43 ± 0.42 (3)	9.27 ± 0.33 (3)	95 ± 5.00 (3)
C27A–C104A	9.29 ± 0.27 (3)	>6.00 (3)	ND
C40A–C57A	9.65 ± 0.11 (3)	>6.00 (3)	ND
C40A–C72A	9.34 ± 0.85 (3)	8.83 ± 0.25* (3)	87 ± 6.00 (3)
C40A–C82A	9.27 ± 0.52 (3)	>6.00 (3)	ND
C40A–C104A	9.23 ± 0.34 (3)	>6.00 (3)	ND
C57A–C72A	9.10 ± 0.22 (3)	>6.00 (3)	ND
C57A–C82A	9.53 ± 0.11 (3)	>6.00 (3)	ND
C57A–C104A	9.12 ± 0.58 (3)	8.10 ± 0.15** (3)	76 ± 5.00 (3)
C72A–C82A	9.11 ± 0.13 (3)	>6.00 (3)	ND
C72A–C104A	9.75 ± 0.17 (3)	>6.00 (3)	ND
C82A–C104A	9.19 ± 0.27 (3)	>6.00 (3)	ND

Values are mean ± SE; number of determinations is shown in parentheses. Significantly different from WT at $P < 0.05$ (*) or $P < 0.001$(***), as assessed by one-way ANOVA with repeated measures followed by Tukey's test. E_{max} is the maximum response expressed as a percentage of the response to the WT. ND, not determined. Comparisons were only made between WT and mutant data from concomitantly transfected cells. A control WT experiment was included in every experiment.

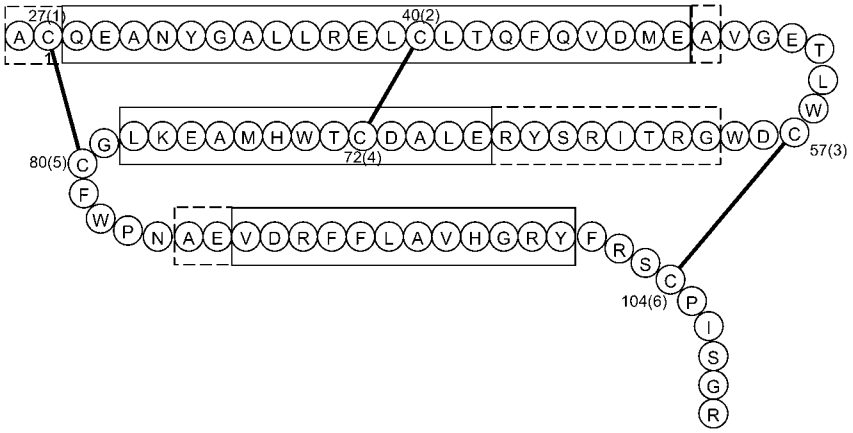

FIGURE 2 Primary sequence of extracellular residues (26–109) of hRAMP1. Shown on the diagram are the consensus α-helical regions (*dotted*) as predicted by JPED and SAMT02 servers and the final positions of the helices (*solid*) after MD refinement. Also shown on the diagram is the disulphide pattern $Cys^{27(1)}$-$Cys^{82(5)}$, $Cys^{40(2)}$-$Cys^{72(4)}$ and $Cys^{57(3)}$-$Cys^{104(6)}$ as suggested by in silico prediction and confirmed by mutagenesis.

mutations C27A, C40A, C57A, C72A, C82A, and C104A. These were subsequently expressed in COS-7 cells, which had no endogenously expressed RAMP1 and their pharmacological characteristics assessed (Table 1 and Fig. 3). The single Ala substitutions to Cys^{27} and Cys^{82} were well-tolerated and resulted in WT-like pEC_{50} values. However, the substitutions to Cys^{40}, Cys^{57}, Cys^{72}, and Cys^{104} resulted in a significantly reduced pEC_{50} value compared to WT (Table 1). Visual inspection of these data revealed three different patterns of signaling which could be classified as i), WT-like; ii), intermediate decrease in potency; and iii), large decrease in potency. This is entirely consistent with a disulfide bonding pattern of 1–5, 2–4, and 3–6 (Fig. 3) which was the computational disulfide bonding prediction. This disulfide bond arrangement was further tested by the generation of three double Cys substitutions (C27A/C82A, C40A/C72A, and C57A/C104A). Interestingly, the pEC_{50} for the double mutations was reduced only by the same extent as observed for the corresponding single mutations (Table 1). To ensure that the absence of an increased effect for the double mutations compared to the individual Cys substitutions was not a system artifact, 12 further double Cys mutations were generated (Table 1). These double Cys mutants sampled all remaining possible disulfide bond pairings. However, these mutant constructs were unable to generate an agonist-induced intracellular response (Table 1). Overall, these data provide evidence that the disulfide bonding pattern in hRAMP1 is 1–5, 2–4, and 3–6.

Model building

Information gained from the secondary structure predictions and the mutagenic data was used as restraints for the ab initio modeling of hRAMP1. Several attempts to use existing ab initio modeling methods to generate hRAMP1 structure were unsuccessful and unable to generate structures which were consistent with the disulfide bonding pattern indicated by our mutagenesis studies. Furthermore, no suitable templates were found using web-based searches such as 3DJURY (34) for construction of homology models. We have therefore

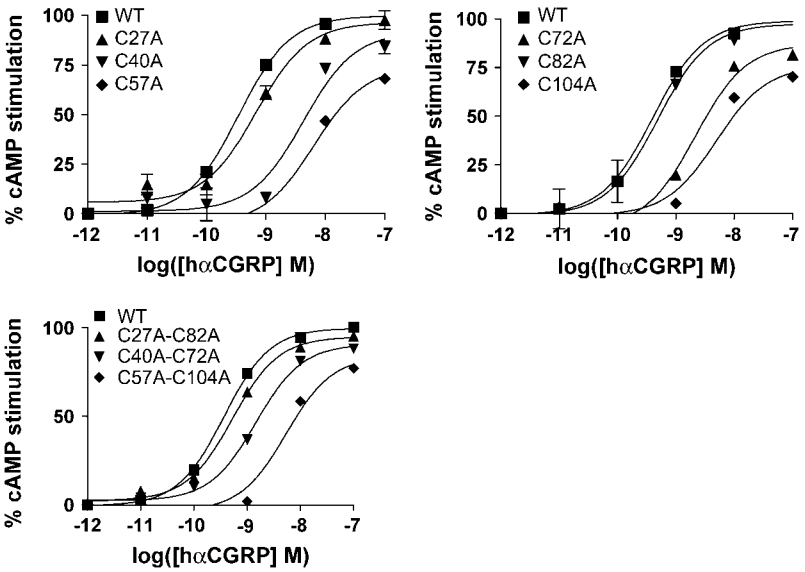

FIGURE 3 CGRP-stimulated cAMP production in mutated RAMPs. Cos 7 cells were transfected with CL/WT hRAMP1 or CL/mutant hRAMP1 and assayed for CGRP-stimulated cAMP production. (■) WT type receptors. Mutant receptors are as indicated. Data are representative of three similar experiments. Points are the mean ± SE of triplicate determinations.

developed an ab initio modeling protocol which was able to include information such as disulfide bonding information and secondary structure to generate an initial ensemble of structures which were scored using a two-tier approach. The lowest energy structure was then further refined using MD.

To assess the effectiveness of an ab initio modeling method, it must be shown to be able to predict the conformation of proteins whose structure has been solved at high resolution. Three helical disulfide containing peptides (PDB:1HP8, PDB:1V54, and PDB:1T0P) from the SCOP database (http://scop.mrc-lmb.cam.ac.uk/scop/) were randomly picked to test the method. Some 25,000 initial decoy structures were generated using information gained from secondary structure prediction and disulfide bonding patterns. Importantly, no information was used from the x-ray crystal structures. These were scored using the RAPDF potential function (28). The top 1000 lowest energy conformations were retained and energy minimized using the AMBER99 force field as implemented in TINKER (29). Visual inspection of the resulting structures revealed that the best 20 lowest energy structures converged onto a single conformation for the modeled structures for PDB:1HP8, PDB:1V54, and PDB:1T0P. These intermediate ab initio structures were compared to the corresponding x-ray crystal coordinates and revealed that the C_α root mean-squared deviation (RMSD) was 5.28 Å, 4.8 Å, and 5.4 Å for PDB:1HP8, PDB:1V54 chain H (residues 21–85), and PDB:1T0P, respectively. This demonstrated that the use of the AMBER/GBSA energy function resulted in the selection of an ab initio model with a fold that was close to the native structure. Further refinement of these intermediate structures was achieved through the use of 50 ns MD simulations which generated an improved structure that exhibited a C_α RMSD of 3.8 Å, 4.1 Å, and 4.0 Å when compared to the x-ray crystal structures PDB:1HP8, PDB:1V54 chain H (residues 21–85), and PDB:1T0P, respectively (Fig. 4).

The validated ab initio approach was then used to generate a structural model for hRAMP1. Initial model building utilized information gained from secondary structure predictions and the experimentally confirmed disulfide bonding pattern. In addition, a further set of decoy structures were generated which utilized the secondary structure prediction information but only used the disulfide pattern of 2–4 and 3–6 as restraints. This step was performed as the mutations C27A and C82A did not perturb intracellular signaling. For both sets of conditions 25,000 decoys were generated and the results compared; both generated similar sets of low energy structures. The best of these were then refined further using the same MD protocol as applied to the ab initio models of the three control peptides of known structure cited above. In the resulting structure (Fig. 5), the three α-helices were retained which confirmed the initial secondary structure prediction, however the start and end points of the α-helices as well as their positioning with respect to one another, were different from the initial conformation. Interestingly, the structures from the two sets of initial disulfide bonding conditions converged to a single structure.

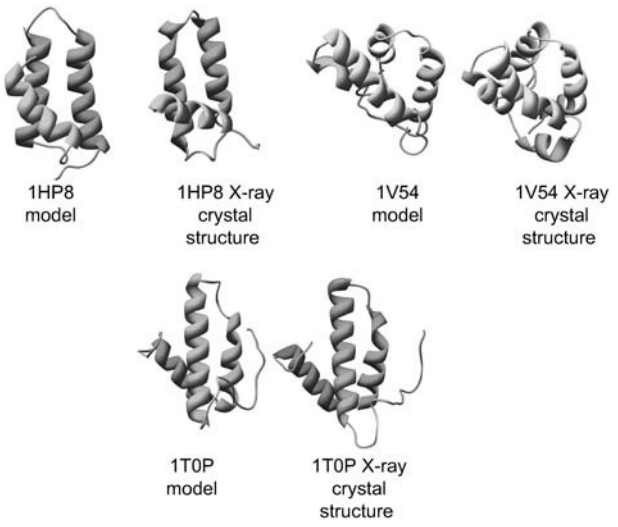

FIGURE 4 Comparison of the refined ab initio models (*left*) and the corresponding x-ray crystal structure (*right*) for PDB:1HP8, PDB:1V54 and PDB:1T0P after 50ns of MD simulation. The structures were compared and revealed a C_α RMSD of 3.8 Å, 4.1 Å, and 4.0 Å for the PDB:1HP8, PDB:1V54, and PDB:1T0P x-ray crystal structures, respectively.

DISCUSSION

In this study, we present a structure for hRAMP1 obtained by molecular modeling which is supported by pharmacological characterization of mutant hRAMP1 constructs. Furthermore, the approaches presented in this study are likely to have widespread utility for studying cysteine-containing peptides in general.

A key step in determining the structure of any cysteine-containing protein is to establish the disulfide bonding

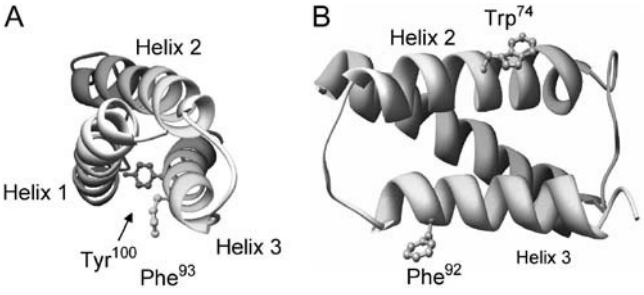

FIGURE 5 Ab initio model of hRAMP1. Panels *A* and *B* show the architecture of hRAMP1 with three helices and interconnecting loops. (*A*) Previous studies have highlighted Phe^{93} and Tyr^{100} as being important in cell surface expression. The ab initio model of hRAMP1 reveals that these residues are located in a cleft between helix1 and helix3. (*B*) Location of $Phe^{92,}$ which has been shown to affect ligand binding, but has little effect on cell surface expression. Also shown in *B* is the location of Trp^{74}, a residue that has been implicated in the high affinity binding of the non-peptide antagonist BIBN4096BS.

pattern and any molecular model of such proteins has to be consistent with this information. Although the effect of mutating individual cysteines in RAMP1 has been reported (12), the disulfide bonding pattern was unknown before this study. To establish the disulfide bonding pattern of RAMP1, it was necessary to undertake systematic Cys substitution, to produce a series of pairwise double Cys mutants. The functional ramifications of these Cys-substituted mutants were then examined for lack of additivity. Lack of an additive effect in double mutants is strong evidence that the two Cys residues contribute to the same bond (35). In this study, our results unambiguously demonstrate that the disulfide bond pattern is 1–5, 2–4, 3–6, which is consistent with a recent abstract using mass spectrometry based analysis (36). Furthermore, it is commonly believed that RAMPs are built from a common architecture (6), therefore this disulfide bonding pattern is likely to be found in the other members of the RAMP family.

This information allowed us to evaluate the various modeling routines that are available to predict disulfide bonding patterns. We used a dataset of disulfide-containing small α-helical proteins of known structure and based on this, selected the neural net-based package, DISULFIND. Not only did this successfully predict the disulfide bond arrangement that was observed experimentally, it also predicted the same pattern for other known RAMP sequences, with the exception of a RAMP precursor from the genus *Tetrodon*. We then extended this approach to select the best secondary structure prediction method. We used a consensus of two methods and again these also predicted that all members of the RAMP family share the same structure; an N-terminus composed of three helices and a single transmembrane helix. The model itself was built using idealized α-helices and systematically sampled the conformational space to identify a low energy bundle. Interestingly, even though a ''brute force'' approach was used to generate the initial structures (for models of both the x-ray crystal structure set and the model of hRAMP1) the two-tiered approach of using the RAPDF score and the AMBER/GBSA force field resulted in structures which were close to the native conformation. In addition, the convergence of the lowest energy structure onto one conformation suggests that the conformational space was adequately sampled by the initial packing search. These structures were refined using an MD protocol described by Fan and Mark (30). In all cases, marked improvement from the initial conformations were observed in the C_α RMSD for the ab initio structures of PDB:1HP8, PDB:1V54, and PDB:1T0P. This suggested that this method was also applicable for the refinement of the hRAMP1 structure, which used the same initial packing protocol. The MD refined structure of hRAMP1 exhibited three α-helices which is consistent with the secondary structure predictions. Furthermore, Fan and Mark (30) also demonstrated that wrongly assigned secondary structure was not stable in their protocols and despite some unraveling of the extreme ends of the hRAMP1 helices, the secondary structure was stable for the 50 ns time lengths of the simulations. In addition to using the disulfide constraints of 1–5, 2–4, and 3–6 we also employed the disulfide bonding pattern of 2–4 and 3–6 in ab initio model building. This revealed that the loss of the 1–5 disulfide restraint had little effect on the conformation of the lowest energy structure and that the loss of the disulfide bond between Cys^{27} and Cys^{82} has little effect on the ab initio folding landscape of hRAMP1. Furthermore, refinement for both sets of disulfide bond arrangements for hRAMP1 modeling (disulfide bonds between Cys 1–5, 2–4, 3–6 versus disulfide bonds between Cys 2–4 and 3–6) converged onto a single conformation. This reveals that a disulfide bond between Cys1–5 does not greatly affect the tertiary fold of the RAMP1 protein and thereby provides the molecular basis underlying the wild-type characteristics of the C27A, C82A, and C27A/C82A mutant RAMP1 constructs.

It is possible to use the model of RAMP1 to examine previous mutagenesis studies reported by others. The most detailed work on structure-function relationships for RAMP1 was carried out by Kuwasako and colleagues (10), who identified residues 91–103 as particularly important. This essentially corresponds to helix 3 in our model structure (Fig. 5). Mutations of Phe^{93}, Tyr^{100}, and Phe^{101} to Ala significantly reduced cell-surface expression of RAMP1; by contrast L94A increased surface expression, most likely due to relief of steric hindrance. The mutants F92A and H97A showed reasonable expression but reduced CGRP binding. Mutation of the other residues in this segment to Ala (Arg^{91}, Val^{96}, Arg^{99}, Arg^{102}, and Ser^{103}) was without effect on binding or expression. Using our model of RAMP1 to interpret the effect of these point mutations revealed that almost all of the residues that alter expression, or CGRP binding, face into the groove between the three helices. Consequently, it is possible that these residues may contribute to the packing of the helices of RAMP1 and thus its stability. However, RAMP1 requires heterodimerization with CLR for cell surface expression (37). Thus it is possible that these residues are required for a binding site between the RAMP and CLR. It has been suggested that the increase in surface expression seen with L94A is due to relief of steric hindrance between the Leu side chain and CLR. In our model, Leu^{94} could interact with a portion of CLR that packed into the interhelical groove. F92A, however (reduced binding of CGRP but WT-like cell-surface expression of RAMP1) is faced away from the groove and could conceivably interact directly with CGRP. It should be noted that in the study by Kuwasako and colleagues (10), CGRP binding was only assessed at a single concentration of radioligand, used well below its K_d; thus the small (twofold) reduction in binding seen with F92A (and H97A) could have been due to an altered K_d. In a separate study, Trp^{74} was identified as a key residue for the binding of the nonpeptide antagonist BIBN4096BS (11). Although Trp^{74} is located on helix 2, it

nevertheless faces in the same direction as Phe^{92}, consistent with a role for these residues in ligand binding (38).

Although RAMP1 is not glycosylated, RAMP3 has four potential glycosylation sites (Fig. 1). Given that the modeling indicates that the two proteins should have essentially similar structures, it is not unreasonable to predict that the equivalent positions to the RAMP3 glycosylation sites (Gln^{28}, Asp^{58}, Asp^{71}, and Ser^{103} of RAMP1) should also be sterically suitable for glycosylation in RAMP1. Indeed, mutating the latter three residues to asparagines produces glycosylation-competent forms of RAMP1 (39). In the model, all of the residues are in sterically unconstrained positions that could readily accommodate carbohydrate chains. The location of Asp^{71} with respect to the critical Trp^{74} is interesting; the side chain of Trp^{74} is predicted to project below that of Asp^{71} so that it is closer to the plasma membrane. Furthermore it points away from Asp^{71} by an angle of $\sim 90°$. Thus, Trp^{74} could interact either directly with BIBN4096BS or with another part of CLR without any interference from carbohydrate.

In conclusion we have generated an ab initio model of hRAMP1 which is consistent with mutagenic data presented above and also provides a rational mechanistic explanation of data published by others. This is the first investigation into a plausible model of hRAMP1 and the data obtained may be applicable to other members of the RAMP family.

This work was supported by grants from the Wellcome Trust and the Biotechnology and Biological Sciences Research Council of the UK (C20090) to D.R.P. and M.W. D.L.H. was supported by the Auckland Medical Research Foundation and the New Zealand Lottery Health fund.

REFERENCES

1. Prinster, S. C., C. Hague, and R. A. Hall. 2005. Heterodimerization of g protein-coupled receptors: specificity and functional significance. *Pharmacol. Rev.* 57:289–298.
2. McLatchie, L. M., N. J. Fraser, M. J. Main, A. Wise, J. Brown, N. Thompson, R. Solari, M. G. Lee, and S. M. Foord. 1998. RAMPs regulate the transport and ligand specificity of the calcitonin-receptor-like receptor. *Nature.* 393:333–339.
3. Christopoulos, G., K. J. Perry, M. Morfis, N. Tilakaratne, Y. Gao, N. J. Fraser, M. J. Main, S. M. Foord, and P. M. Sexton. 1999. Multiple amylin receptors arise from receptor activity-modifying protein interaction with the calcitonin receptor gene product. *Mol. Pharmacol.* 56:235–242.
4. Christopoulos, A., G. Christopoulos, M. Morfis, M. Udawela, M. Laburthe, A. Couvineau, K. Kuwasako, N. Tilakaratne, and P. M. Sexton. 2003. Novel receptor partners and function of receptor activity-modifying proteins. *J. Biol. Chem.* 278:3293–3297.
5. Bouschet, T., S. Martin, and J. M. Henley. 2005. Receptor-activity-modifying proteins are required for forward trafficking of the calcium-sensing receptor to the plasma membrane. *J. Cell Sci.* 118:4709–4720.
6. Hay, D. L., D. R. Poyner, and P. M. Sexton. 2006. GPCR modulation by RAMPs. *Pharmacol. Ther.* 109:173–197.
7. Fraser, N. J., A. Wise, J. Brown, L. M. McLatchie, M. J. Main, and S. M. Foord. 1999. The amino terminus of receptor activity modifying proteins is a critical determinant of glycosylation state and ligand binding of calcitonin receptor-like receptor. *Mol. Pharmacol.* 55:1054–1059.
8. Zumpe, E. T., N. Tilakaratne, N. J. Fraser, G. Christopoulos, S. M. Foord, and P. M. Sexton. 2000. Multiple ramp domains are required for generation of amylin receptor phenotype from the calcitonin receptor gene product. *Biochem. Biophys. Res. Commun.* 267:368–372.
9. Kuwasako, K., K. Kitamura, K. Ito, T. Uemura, Y. Yanagita, J. Kato, T. Sakata, and T. Eto. 2001. The seven amino acids of human RAMP2 (86) and RAMP3 (59) are critical for agonist binding to human adrenomedullin receptors. *J. Biol. Chem.* 276:49459–49465.
10. Kuwasako, K., K. Kitamura, Y. Nagoshi, Y. N. Cao, and T. Eto. 2003. Identification of the human receptor activity-modifying protein 1 domains responsible for agonist binding specificity. *J. Biol. Chem.* 278:22623–22630.
11. Mallee, J. J., C. A. Salvatore, B. LeBourdelles, K. R. Oliver, J. Longmore, K. S. Koblan, and S. A. Kane. 2002. Receptor activity-modifying protein 1 determines the species selectivity of non-peptide CGRP receptor antagonists. *J. Biol. Chem.* 277:14294–14298.
12. Steiner, S., W. Born, J. A. Fischer, and R. Muff. 2003. The function of conserved cysteine residues in the extracellular domain of human receptor-activity-modifying protein. *FEBS Lett.* 555:285–290.
13. Boussif, O., F. Lezoualc'h, M. A. Zanta, M. D. Mergny, D. Scherman, B. Demeneix, and J. P. Behr. 1995. A versatile vector for gene and oligonucleotide transfer into cells in culture and in vivo: polyethylenimine. *Proc. Natl. Acad. Sci. USA.* 92:7297–7301.
14. Poyner, D. R. 1992. Calcitonin gene-related peptide: multiple actions, multiple receptors. *Pharmacol. Ther.* 56:23–51.
15. Murzin, A. G., S. E. Brenner, T. Hubbard, and C. Chothia. 1995. SCOP: a structural classification of proteins database for the investigation of sequences and structures. *J. Mol. Biol.* 247:536–540.
16. Cuff, J. A., M. E. Clamp, A. S. Siddiqui, M. Finlay, and G. J. Barton. 1998. JPred: a consensus secondary structure prediction server. *Bioinformatics.* 14:892–893.
17. Garnier, J., J. F. Gibrat, and B. Robson. 1996. GOR method for predicting protein secondary structure from amino acid sequence. *Methods Enzymol.* 266:540–553.
18. Karplus, K., R. Karchin, J. Draper, J. Casper, Y. Mandel-Gutfreund, M. Diekhans, and R. Hughey. 2003. Combining local-structure, fold-recognition, and new fold methods for protein structure prediction. *Proteins.* 53(Suppl 6):491–496.
19. Rost, B., and C. Sander. 1993. Prediction of protein secondary structure at better than 70% accuracy. *J. Mol. Biol.* 232:584–599.
20. Ouali, M., and R. D. King. 2000. Cascaded multiple classifiers for secondary structure prediction. *Protein Sci.* 9:1162–1176.
21. McGuffin, L. J., K. Bryson, and D. T. Jones. 2000. The PSIPRED protein structure prediction server. *Bioinformatics.* 16:404–405.
22. Vullo, A., and P. Frasconi. 2004. Disulfide connectivity prediction using recursive neural networks and evolutionary information. *Bioinformatics.* 20:653–659.
23. Ferre, F., and P. Clote. 2005. DiANNA: a web server for disulfide connectivity prediction. *Nucl. Acids Res.* 33:W230–232.
24. O'Connor, B. D., and T. O. Yeates. 2004. GDAP: a web tool for genome-wide protein disulfide bond prediction. *Nucl. Acids Res.* 32:W360–364.
25. Cheng, J., A. Z. Randall, M. J. Sweredoski, and P. Baldi. 2005. SCRATCH: a protein structure and structural feature prediction server. *Nucl. Acids Res.* 33:W72–76
26. Tsai, C.-H., B.-J. Chen, C.-h. Chan, H.-L. Liu, and C.-Y. Kao. 2005. Improving disulfide connectivity prediction with sequential distance between oxidized cysteines. *Bioinformatics.* 21:4416–4419.
27. Bower, M. J., F. E. Cohen, and R. L. Dunbrack, Jr. 1997. Prediction of protein side-chain rotamers from a backbone-dependent rotamer library: a new homology modeling tool. *J. Mol. Biol.* 267:1268–1282.
28. Samudrala, R., and J. Moult. 1998. An all-atom distance-dependent conditional probability discriminatory function for protein structure prediction. *J. Mol. Biol.* 275:895–916.
29. Pappu, R. V., G. R. Marshall, and J. W. Ponder. 1999. A potential smoothing algorithm accurately predicts transmembrane helix packing. *Nat. Struct. Biol.* 6:50–55.
30. Fan, H., and A. E. Mark. 2004. Mimicking the action of folding chaperones in molecular dynamics simulations: application to the

refinement of homology-based protein structures. *Protein Sci.* 13: 992–999.

31. Lindahl, E., B. Hess, and D. v. d. Spoel. 2001. GROMACS 3.0: a package for molecular simulation and trajectory analysis. *J. Mol. Model. (Online).* 7:306–317.
32. Feenstra, K. A., B. Hess, and H. J. C. Berendsen. 1999. Improving efficiency of large time-scale molecular dynamics simulations of hydrogen-rich systems. *J. Comput. Chem.* 20:786–798.
33. Kahsay, R. Y., G. Gao, and L. Liao. 2005. An improved hidden Markov model for transmembrane protein detection and topology prediction and its applications to complete genomes. *Bioinformatics.* 21:1853–1858.
34. Ginalski, K., A. Elofsson, D. Fischer, and L. Rychlewski. 2003. 3D-Jury: a simple approach to improve protein structure predictions. *Bioinformatics.* 19:1015–1018.
35. Lee, W. Y., and S. M. Sine. 2005. Principal pathway coupling agonist binding to channel gating in nicotinic receptors. *Nature.* 438:243–247.
36. Chang, C. L., R. C. Winant, and S. Y. T. Hsu. 2005. Select disulfide bridges in the receptor activity modifying protein 1 (RAMP1) ectodomain are essential for RAMP1/CRLR receptor signalling. *Proc. Experimental Biology.* 795.4. http://www.faseb.org/meetings/eb2005. (Abstr.)
37. Flahaut, M., B. C. Rossier, and D. Firsov. 2002. Respective roles of calcitonin receptor-like receptor (CRLR) and receptor activity-modifying proteins (RAMP) in cell surface expression of CRLR/RAMP heterodimeric receptors. *J. Biol. Chem.* 277:14731–14737.
38. Doods, H., G. Hallermayer, D. Wu, M. Entzeroth, K. Rudolf, W. Engel, and W. Eberlein. 2000. Pharmacological profile of BIBN4096BS, the first selective small molecule CGRP antagonist. *Br. J. Pharmacol.* 129:420–423.
39. Flahaut, M., C. Pfister, B. C. Rossier, and D. Firsov. 2003. N-Glycosylation and conserved cysteine residues in RAMP3 play a critical role for the functional expression of CRLR/RAMP3 adrenomedullin receptor. *Biochemistry.* 42:10333–10341.